International Communications in Heat and Mass Transfer 37 (2010) 1350–1358

Contents lists available at ScienceDirect

International Communications in Heat and Mass Transfer

journal homepage: www.elsevier.com/locate/ichmt

Natural convection in divided trapezoidal cavities filled with fluid saturated porous media ☆

Yasin Varol

Department of Mechanical Education, Firat University, 23119 Elazig, Turkey

ARTICLE INFO

Available online 4 August 2010

Keywords:
Trapezoidal cavity
Natural convection
Conjugate

ABSTRACT

A numerical work was performed to determine the heat transfer and fluid flow due to buoyancy forces in divided trapezoidal enclosures filled with fluid saturated porous media. In the present investigation, bottom wall was non-uniformly heated while two vertical walls were insulated and the top wall was maintained at constant cold temperature. The divider had constant thermal conductivity. Flow patterns and temperature distribution were obtained by solving numerically the governing equations, using Darcy's law. Results are presented for different values of the governing parameters, such as Rayleigh number for a porous medium, location of the partition, thickness of the partition and thermal conductivity ratio between solid and fluid media. It was observed that the conduction mode of heat transfer became dominant inside the cavity for higher thickness of the partition, low Rayleigh numbers, and low thermal conductivity ratio.

1. Introduction

Natural convection heat transfer and fluid flow in porous media was widely investigated in engineering applications such as post-accidental heat removal in nuclear reactors, solar collectors, drying processes, fire control, geophysics, and geothermal applications and so on [1–4]. The problem of buoyancy induced flow in trapezoidal cavity inclined at different angles filled with a viscous fluid was analyzed by Lee [5]. He performed a numerical study of this problem in order to analyze the behavior of the flow and heat transfer characteristics at different Rayleigh *Ra* and Prandtl numbers *Pr* using curvilinear geometry. It was shown that for $Ra>10^4$ and $Pr>0.1$, the heat transfer, in a trapezoidal enclosure with two symmetrical, inclined sidewalls of moderate aspect ratio, was a strong function of the orientation angle of the cavity. Non-isothermal boundary conditions could be seen in metallurgy to obtain regular melting for metal and it can be obtained with a cylindrical heater for laboratory experiment ([6], Saeid [7] and Varol et al. [8]).

Kumar and Kumar [9] analyzed the natural convection heat transfer in a trapezoidal cavity filled with a porous medium by using parallel computation technique. The bottom and top walls were taken as adiabatic and inclined walls were differentially heated. They showed that the inclination of the side wall was an important parameter on the flow and temperature distribution. Baytas and Pop [10] solved the Darcy and energy equations in cylindrical coordinates using ADI method in order to analyze natural convection in a porous trapezoidal enclosure. They indicated that up to Rayleigh number equal to 100, a conduction-dominated regime prevailed, and afterwards a two-cellular convective flow regime took place at the tilt angle 165°. Moukalled and Acharya [11] studied the conjugate natural convection heat transfer in a trapezoidal cavity with a divider attached onto inclined wall. In their case, the cavity was filled with a viscous fluid. Moukalled and Darwish [12] performed a numerical analysis of natural convection in a partitioned trapezoidal cavity using the special momentum-weighted interpolation method. They used conductive short partition/partitions and they showed that the presence of baffles decreased heat transfer as high as 70%. Other similar studies on natural convection in trapezoidal cavities were done by Peric [13], Van Der Eyden et al. [14], Boussaid et al. [15], Kumar [16], Papanicolaou and Belessiotis [17], Hammami et al. [18], Varol et al. [19–21] and Natarajan et al. [22].

The main aim of this study was to examine the natural convection heat transfer, temperature and flow field in a horizontally divided trapezoidal cavity filled with a fluid-saturated porous medium. Streamlines, isotherms, and local and mean Nusselt numbers will be presented in the following sections of the paper for different Rayleigh numbers, thermal conductivity ratio, thickness of the partition, and location of the partition.

2. Considered model

The physical model is drawn in Fig. 1 (a). This figure also shows the coordinates and boundary conditions. The system was a

☆ Communicated by W.J. Minkowycz.
E-mail address: ysnvarol@gmail.com.

0735-1933/$ – see front matter © 2010 Elsevier Ltd. All rights reserved.
doi:10.1016/j.icheatmasstransfer.2010.07.010

Nomenclature

g	gravitational acceleration
h'	location of partition in the y-direction
h	dimensionless location of partition in the y-direction, $(h=h'/H)$
H	height of the cavity, $H=L/2$
k_f	thermal conductivity of the fluid
k_s	thermal conductivity of the solid partition
k	thermal conductivity ratio, (k_s/k_f)
K	permeability of the porous medium
L	length of the bottom wall of the enclosure
ℓx	dimensionless length of the under surface of the partition, $\ell x'/L$
ℓx_u	dimensionless length of the upper surface of the partition, $\ell x_u'/L$
n	coordinate in normal direction
Nu	local Nusselt number
Nu_m	mean Nusselt number
Pr	Prandtl number
Ra	Rayleigh number for a porous medium
t'	thickness of the solid partition
t	dimensionless thickness of the solid partition, $(t=t'/H)$
T	temperature
u,v	dimensional axial and radial velocities
X,Y	non-dimensional coordinates

Greek letters

α_m	effective thermal diffusivity of the porous medium
β	thermal expansion coefficient
γ	inclination angle of side walls, $(\gamma=35°)$
θ	non-dimensional temperature
υ	kinematic viscosity
Ψ	non-dimensional stream function

Subscript

c	cold
f	fluid
h	hot
s	solid

trapezoidal cavity filled with a fluid saturated porous medium. A horizontal partition separated the cavity into two different parts. It had a conductive material. The inclination angle of the trapezoidal cavity was 35°. Thus, the change of the length of partition depended on its location on y-axis. The length of the bottom wall was L and the height of the cavity was $H=L/2$. The change of the temperature of the bottom wall was non-uniform with a cosine function while two vertical walls were adiabatic and the top wall was maintained at constant cold temperature.

3. Equations and their numerical solution

Governing equations are written as follows:

$$\frac{\partial u}{\partial x}+\frac{\partial v}{\partial y}=0 \tag{1}$$

$$\frac{\partial u}{\partial y}-\frac{\partial v}{\partial x}=-\frac{g\beta K}{\upsilon}\frac{\partial T_f}{\partial x} \tag{2}$$

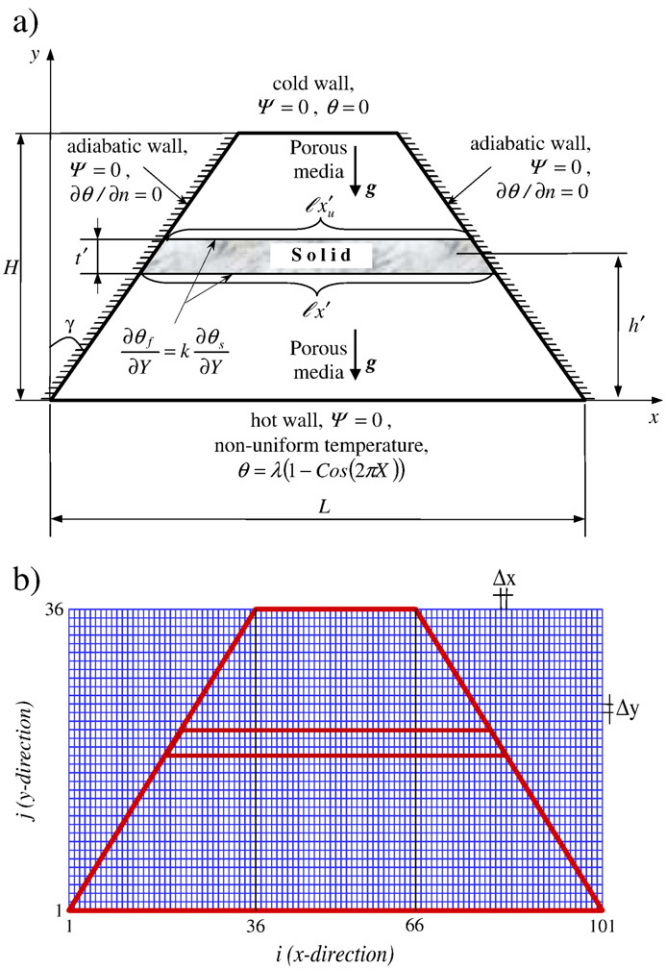

Fig. 1. a) Physical model and b) finite-difference grid for a trapezoidal enclosure.

$$u\frac{\partial T_f}{\partial x}+v\frac{\partial T_f}{\partial y}=\alpha_m\left(\frac{\partial^2 T_f}{\partial x^2}+\frac{\partial^2 T_f}{\partial y^2}\right) \tag{3}$$

and the energy equation for the solid partition wall is:

$$\frac{\partial^2 T_s}{\partial x^2}+\frac{\partial^2 T_s}{\partial y^2}=0. \tag{4}$$

To write the given equations the assumptions are listed as follows:

- the properties of the fluid and the porous medium are constant,
- the cavity walls are impermeable,
- the Boussinesq approximation and the Darcy law model are valid, and
- the viscous drag and inertia terms in the Darcy and energy equations are negligible.

In the equations, u and v are the velocity components along x and y axes, T_f is the fluid temperature, g is the acceleration due to gravity, T_s is the temperature of the solid partition wall, K is the permeability of the porous medium, α_m is the effective thermal diffusivity of the porous medium, β is the thermal expansion coefficient and υ is the kinematic viscosity. Introducing the stream function ψ defined as

$$u=\frac{\partial \psi}{\partial y},\quad v=-\frac{\partial \psi}{\partial x}. \tag{5}$$

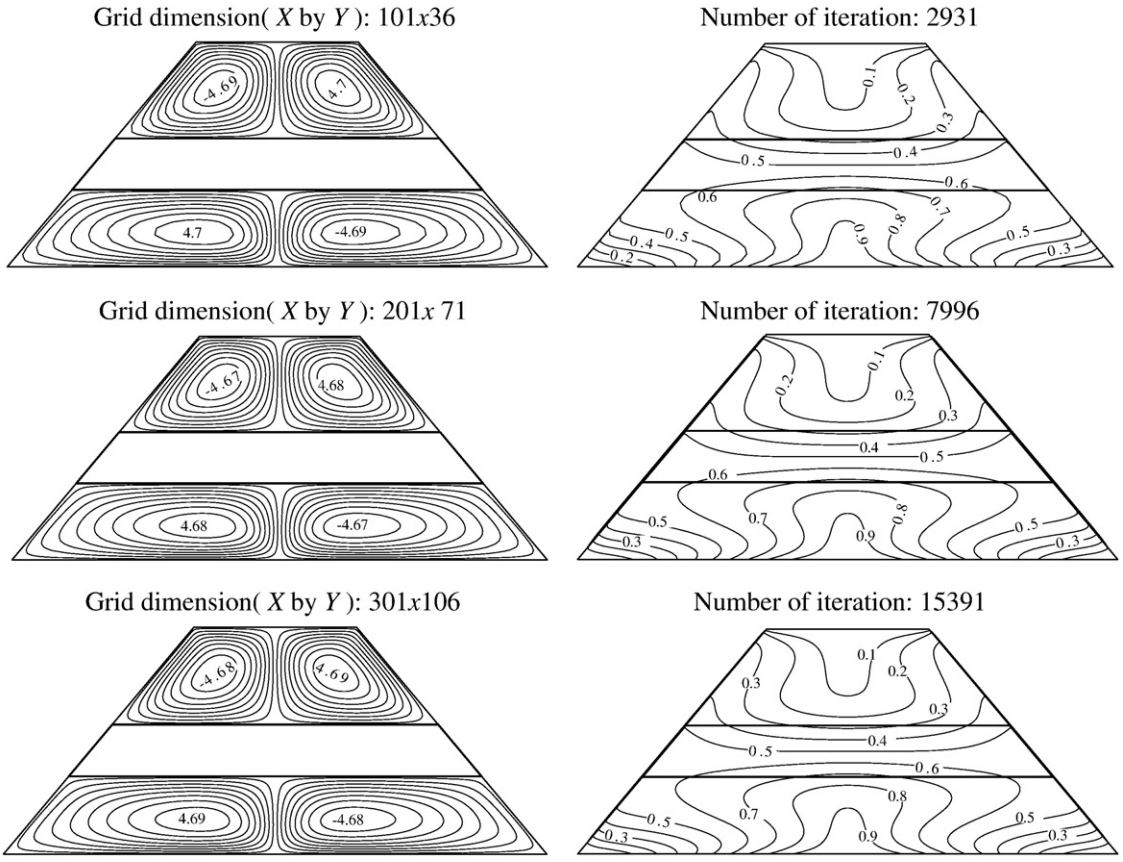

Fig. 2. Grid independency test at $t=0.2$, $h=0.45$, $k=1$, and $Ra=1000$.

Eqs. (1–4) can be written in non-dimensional form as

$$\frac{\partial^2\Psi}{\partial X^2}+\frac{\partial^2\Psi}{\partial Y^2}=-Ra\frac{\partial\theta_f}{\partial X} \tag{6}$$

$$\frac{\partial\Psi}{\partial Y}\frac{\partial\theta_f}{\partial X}-\frac{\partial\Psi}{\partial X}\frac{\partial\theta_f}{\partial Y}=\frac{\partial^2\theta_f}{\partial X^2}+\frac{\partial^2\theta_f}{\partial Y^2} \tag{7}$$

for the fluid-saturated porous medium and

$$\frac{\partial^2\theta_s}{\partial X^2}+\frac{\partial^2\theta_s}{\partial Y^2}=0 \tag{8}$$

for the solid partition wall, respectively. Here $Ra=g\beta K(T_h-T_c)L/\alpha_m\upsilon$ is the Rayleigh number for the porous medium and the non-dimensional quantities are defined as

$$X=\frac{x}{L},Y=\frac{y}{L},\Psi=\frac{\psi}{\alpha_m},\theta_f=\frac{T_f-T_c}{T_h-T_c},\theta_s=\frac{T_s-T_c}{T_h-T_c}. \tag{9}$$

The boundary conditions of Eqs. (6–8) are:
for all solid boundaries

$$\Psi=0; \tag{10a}$$

on the bottom wall (hot), non-uniform temperature is applied as

$$\theta_f=\lambda[1-\cos(2\pi X)] \tag{10b}$$

where the value of λ was taken as 0.5;
on the top wall (cold),

$$\theta_f=0; \tag{10c}$$

on the side walls (adiabatic),

$$\frac{\partial\theta_f}{\partial n}=0; \tag{10d}$$

for the interface between solid partition wall and porous medium,

$$k_f\frac{\partial\theta_f}{\partial Y}=k_s\frac{\partial\theta_s}{\partial Y} \tag{10e}$$

where k_f and k_s are the thermal conductivities of the fluid and solid walls, respectively. Physical quantities of interest in this problem are the local Nusselt number Nu and the mean Nusselt number Nu_m, which can be expressed as

Table 1
Comparison of the present results for $Ra=100$.

Inclination angle of the side wall (γ)	15°	30°	45°
Nu_m (Baytas and Pop [25])	2.95	2.62	2.23
Nu_m (present study)	2.872	2.585	2.217

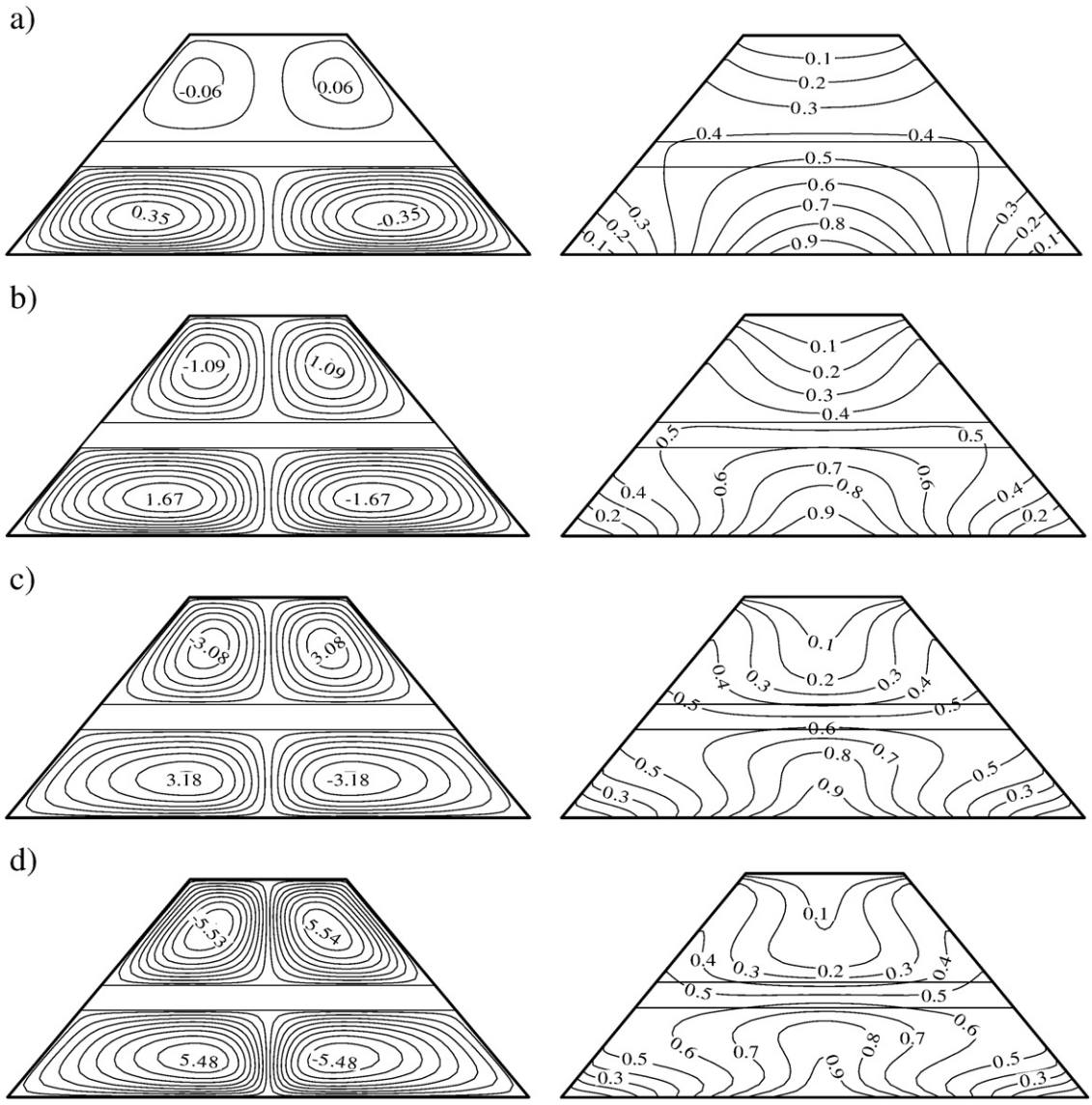

Fig. 3. Streamlines (left) and isotherms (right) for different Rayleigh numbers at $t=0.1$ and $h=0.45$: a)$Ra=50$, b)$Ra=250$, c)$Ra=500$, d)$Ra=1000$.

on the bottom wall:

$$Nu = \left(-\frac{\partial\theta_f}{\partial Y}\right)_{Y=0}, \quad Nu_m = \int_0^1 Nu\, dX; \tag{11a, b}$$

under surface of the partition:

$$Nu = \left(-\frac{\partial\theta_f}{\partial Y}\right)_{Y=h-t/2}, \quad Nu_m = \frac{1}{\ell x}\int_0^{\ell x} Nu.dx; \text{ and} \tag{12a, b}$$

upper surface of the partition:

$$Nu = \left(-\frac{\partial\theta_f}{\partial Y}\right)_{Y=h+t/2}, \quad Nu_m = \frac{1}{\ell x_u}\int_0^{\ell x_u} Nu.dx \tag{13a, b}$$

for the interface between the solid partition and the porous medium.

Eqs. (6–8) were solved numerically with finite-difference method. Numerical simulations were carried out systematically in order to determine the effects of effective parameters of the problem as Rayleigh number Ra, thermal conductivity ratio $k(=k_s/k_f)$, dimensionless thickness of the solid partition wall $t(=t'/H)$ and dimensionless location of partition in the y-direction $h(=h'/H)$ on the flow and heat transfer characteristics. To solve the equations on inclined boundaries, the technique of Asan and Namli [23] and Haese and Teubner [24] were followed. The used mesh treatment was depicted in Fig. 1 (b). The uppermost grid-point on each vertical grid line coincided with the top wall of the trapezoidal enclosures. The inclined wall was approximated with staircase-like zigzag lines. A series of tests on grid-independency against the streamlines and isotherms were conducted for $t=0.2$, $h=0.45$, $k=1$ and $Ra=1000$. They are presented in Fig. 2 by streamlines (on the left) and isotherms (on the right). As seen from this figure, the grid sizes of101×36, 201×71 and 301×106 were selected. Iteration numbers also increase with increasing of mesh size. The comparison of figures indicated that there were no big differences on streamlines, isotherms and stream functions among grid dimensions. Thus, the

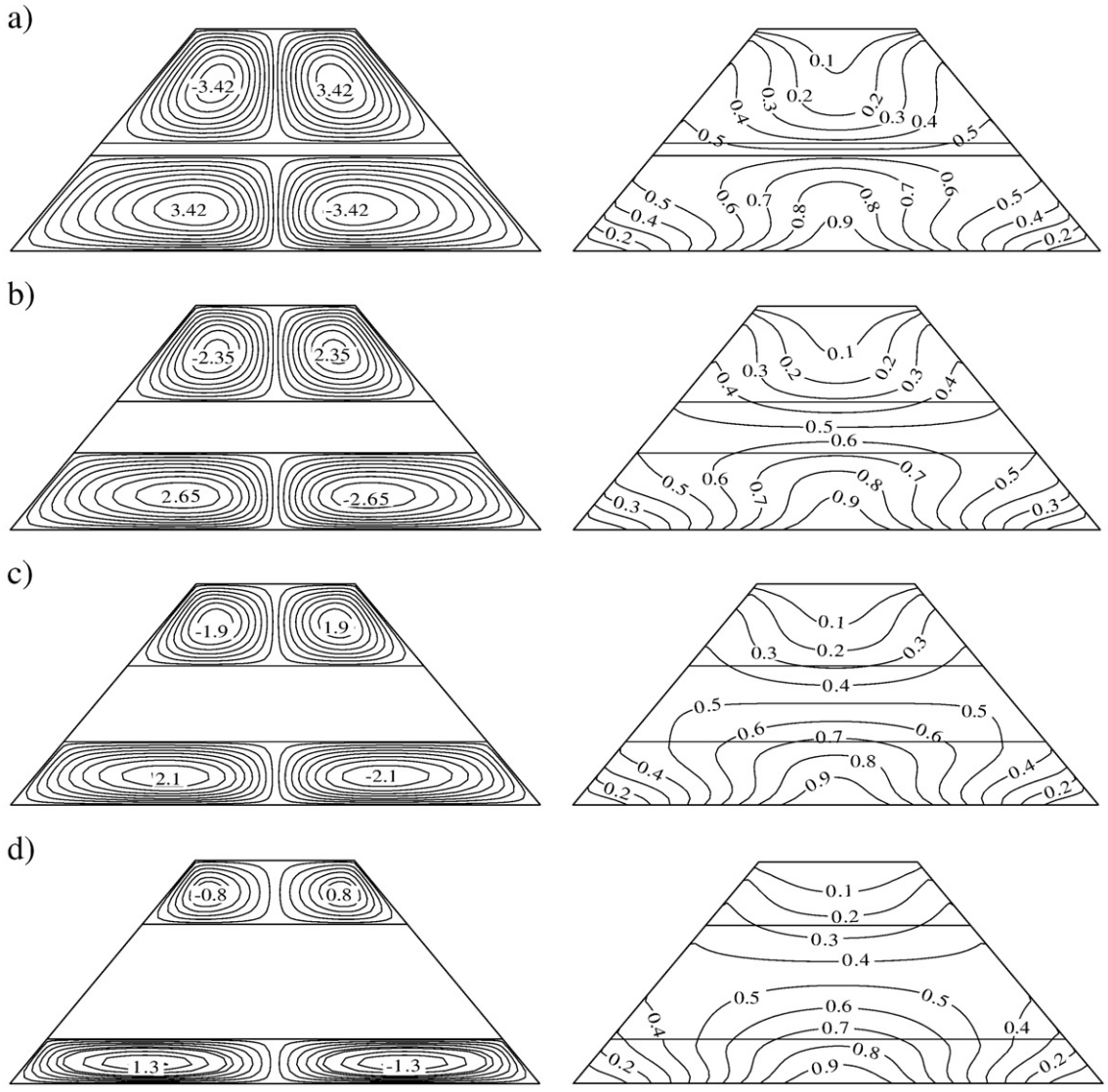

Fig. 4. Streamlines (left) and isotherms (right) for different dimensionless thicknesses of the partition at $h=0.45$, $k=1$ and $Ra=500$: a) $t=0.05$, b) $t=0.2$, c) $t=0.3$, d) $t=0.5$.

grid dimension was considered as 101×36. The iteration process was terminated when the following condition was met

$$\sum_{i,j}\left|\frac{\Phi_{i,j}^{m}-\Phi_{i,j}^{m-1}}{\Phi_{i,j}^{m}}\right|\leq10^{-5} \tag{14}$$

where m denoted the iteration step and Φ stood for either θ_f, θ_s or Ψ.

3.1. Validation of the code

To validate the study, the obtained results were validated against the existing results for a square cavity filled with a porous medium as a first comparison. Thus, the comparison of the present results for the mean Nusselt number Nu_m, as defined by Eq. (11b), with those from the open literature was made for a value of $Ra=1000$. For this, the comparison results can be found in our earlier publications as Varol et al. [8]. The second test was performed to show validation of the code with literature as given in Table 1. In this case, results are compared with the results reported by Baytas and Pop [25], which were for a parallelogram cavity filled with a fluid-saturated porous medium at different inclination angles. As seen from Table 1, the maximum difference between the results by Baytas and Pop [25] and the present results is 0.5%. Thus, the two tests show that the results of the present code are in good agreement with those from the open literature and they can be used with great confidence for further calculations.

4. Results and discussion

In this study, numerical results for streamlines, isotherms, local and mean Nusselt numbers for natural convection in partially divided porous trapezoidal cavity were obtained for Ra numbers, thickness of the horizontal partition, location of the horizontal partition, and thermal conductivity ratio.

Fig. 3 (a) to (d) shows the streamlines (left) and isotherms (right) for different Rayleigh numbers at $t=0.1$, $h=0.45$ and $k=1$. In these figures, four eddies were formed from $Ra=50$ to 1000. These eddies were distributed symmetrically according to middle vertical axis of the cavity. Also, absolute values of streamfunctions were the same at the left and right eddies. It is noticed that eddies above and below of

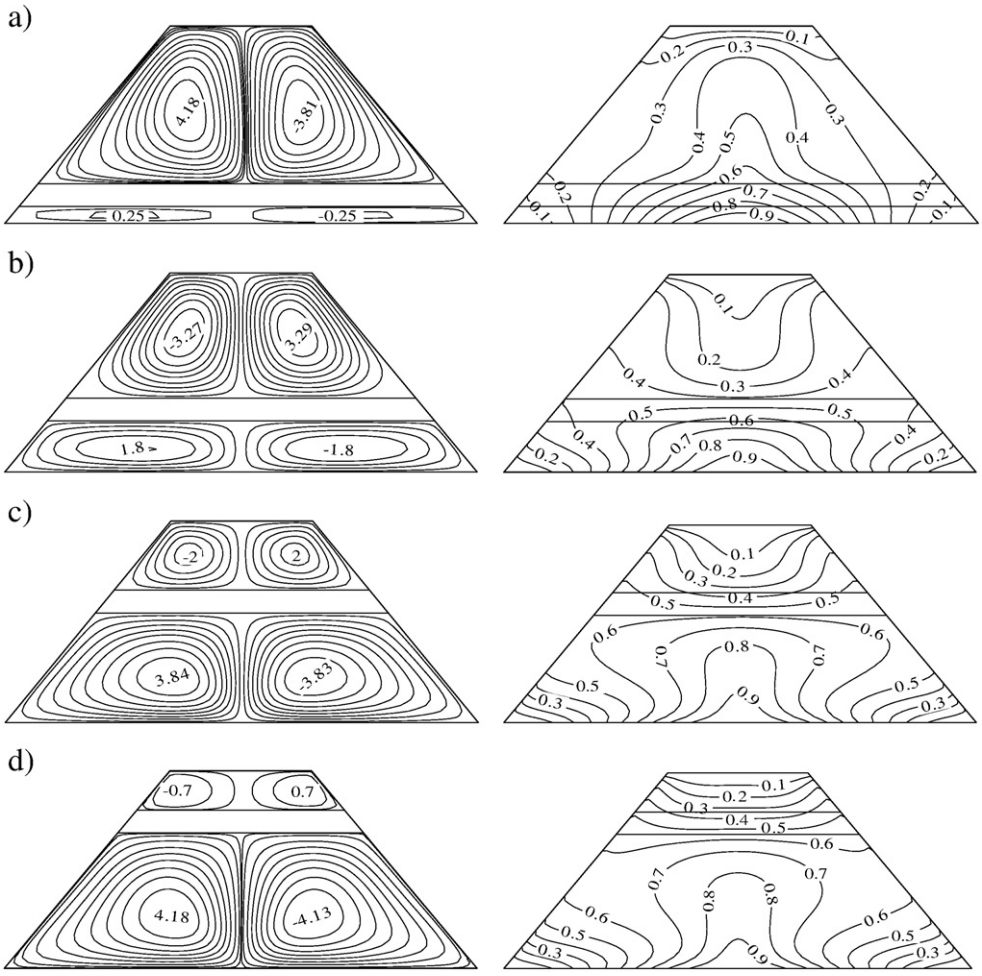

Fig. 5. Streamlines (left) and isotherms (right) for different dimensionless locations of the partition at $t=0.1$, $k=1$ and $Ra=500$: a) $h=0.15$, b)$h=0.30$, c)$h=0.60$, d)$h=0.75$.

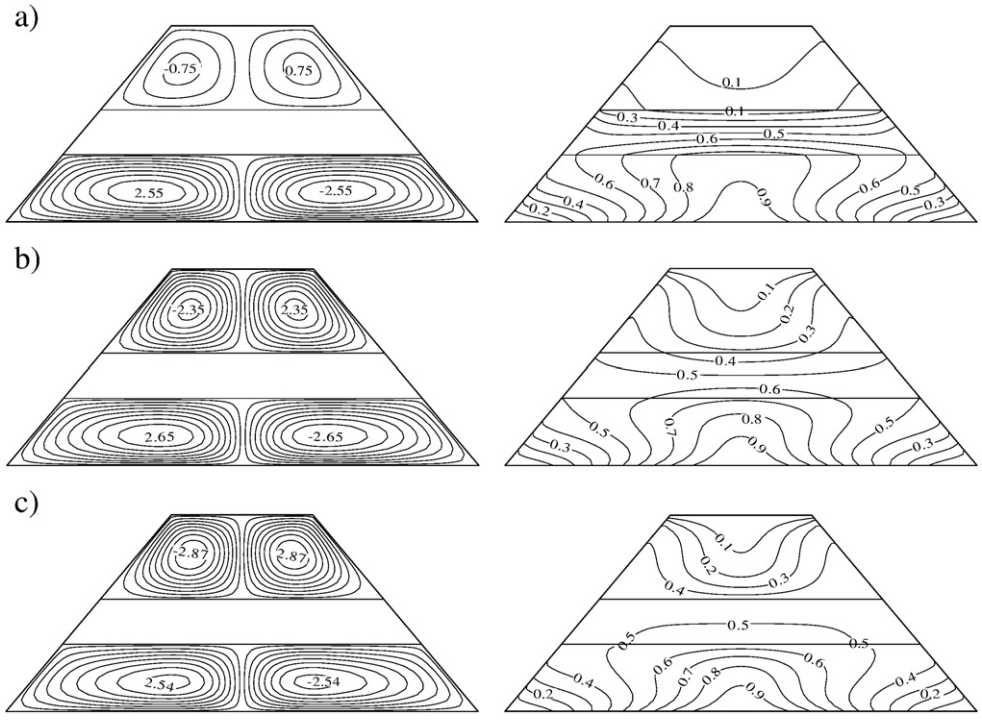

Fig. 6. Streamlines (left) and isotherms (right) for different thermal conductivity ratios at $t=0.2$, $h=0.45$, and $Ra=500$: a) $k=0.1$, b) $k=1$, c) $k=10$.

the partition turned different directions. The right eddy above the fin turned towards clockwise direction. However, the right eddy below the partition turned in counterclockwise. As expected, absolute values of streamfunction were higher for below eddies than that of above eddies for lower Rayleigh number. In this figure, the right column shows the temperature distribution. With increasing of Rayleigh number, the plumelike flow was formed from bottom to top. On the contrary, bowl shaped distribution was observed.

Fig. 4 (a) to (d) illustrates the streamlines (left) and isotherms (right) to show the effects of thickness of partition on flow fields and temperature distribution. The values of thickness changed from $t=0.05$ to $t=0.5$. Increasing of thickness of partition enhanced the domination of conduction mode of heat transfer which was an expected result. Flow strength became weaker with increasing of thickness of partition. As seen from the figure, the number of eddies was independent from the thickness. Convection mode of heat transfer became stronger with increasing of thickness of partition. The reason of this phenomenon was transfer of heat from bottom to top. This can be seen from the isotherms clearly.

The effect of dimensionless location of the partition on flow fields and temperature distribution is shown in Fig. 5 (a) to (d). The location of partition changed from 0.15 to 0.75. The figure shows that the shape of eddies strongly depended on the location of the partition. The flow strength decreased above the partition and increased below

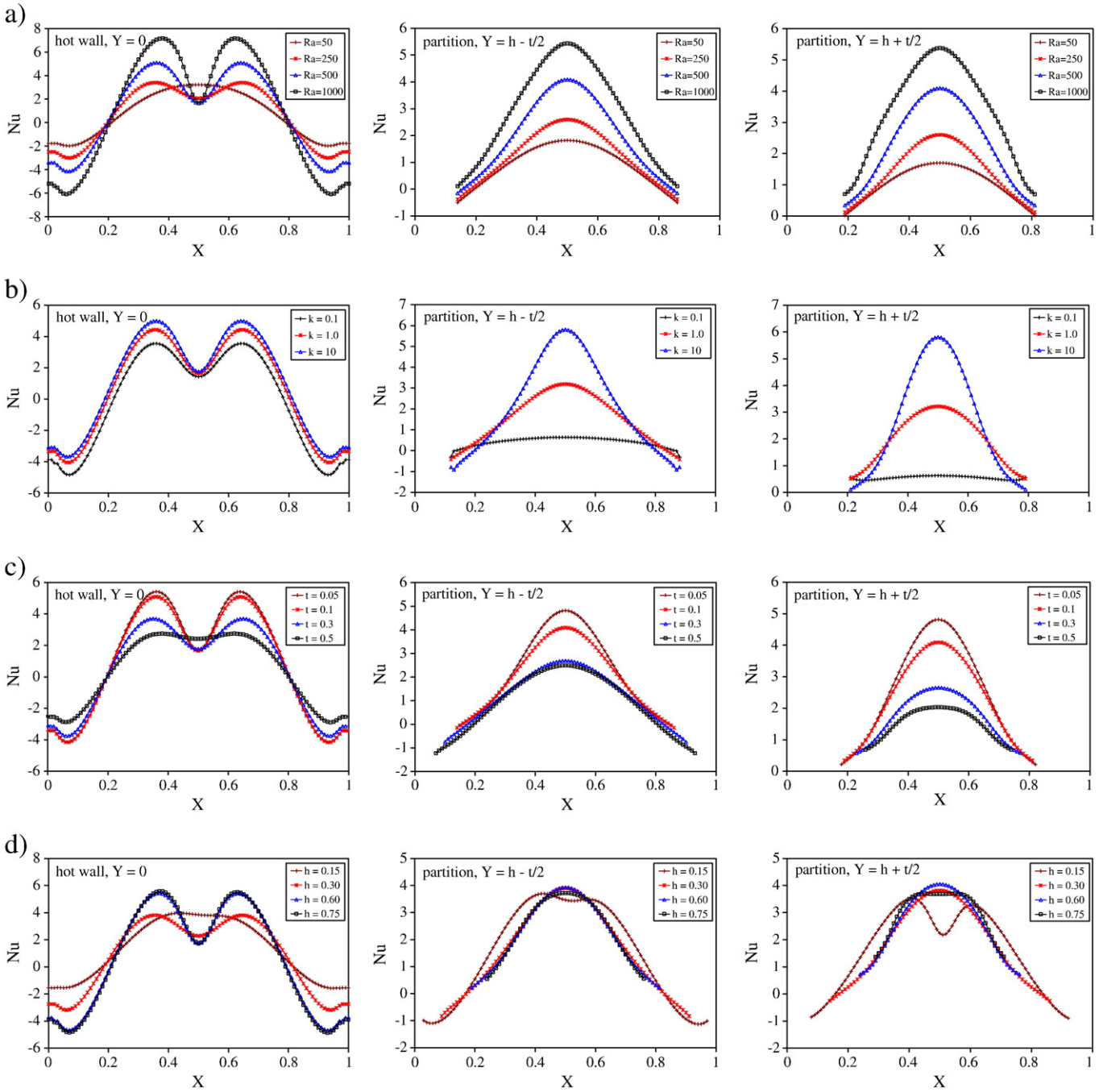

Fig. 7. The variation of local Nusselt numbers along the horizontal walls (along the bottom wall (left), along the bottom side of the partition (middle), and along the upper side of the partition (right)): a) for different Rayleigh numbers at $t=0.1$, $h=0.45$, and $k=1$; b) for different thermal conductivity ratios at $t=0.2$, $h=0.45$, and $Ra=500$; c)for different dimensionless thicknesses of the partition at $h=0.45$, $k=1$, and $Ra=500$; and d) for different dimensionless locations of the partition at $t=0.1$, $k=1$, and $Ra=500$.

the partition with increasing of location of the partition. It was an interesting result that the direction of eddy was the same at left and right for minimum value of location. For this case, plumelike distribution of isotherms was formed for the whole cavity. On the contrary, bowl shaped distribution was formed for higher value of location of the partition.

Fig. 6 (a) to (c) illustrates the effects of thermal conductivity for $t=0.2$, $h=0.45$ and $Ra=500$ on flow fields and temperature distribution by plotting streamlines and isotherms, respectively. The results were given for the values of thermal conductivity from $k=0.1$ to $k=10$. In the case, the flow strength increased with increasing of thermal conductivity values above the partition. More flow was heated under the partition. For $k=0.1$, the partition behaved as an insulation material. It was an interesting result that flow strength became weaker for higher values of thermal conductivity.

Fig. 7 (a) presents the variation of the local Nusselt number along the bottom wall (left), along the bottom side of the partition (middle) and along the top side of the partition (right) for different Rayleigh numbers at $t=0.1$, $h=0.45$, and $k=1$. In the same manner, the local Nusselt number was presented for different values of thermal conductivity. As can be seen from the figures, distribution of local Nusselt number was completely symmetric according to the middle axis of the bottom wall. Due to domination of conduction mode of heat transfer, bell-shaped distribution was formed at $Ra=50$. However, there was a minimal point at the middle of the bottom wall due to the motionless fluid at that part. On the bottom wall of the trapezoidal enclosure, heat transfer increased with increasing of thermal conductivity as seen from Fig. 7 (b) (on the left). Heat transfer was almost constant for $k=0.1$ along the bottom and top sides of the partition. Fig. 7 (c) and (d) presents the local Nusselt number for different thicknesses of the partition and location of the partition, respectively. As seen from these figures, the local Nusselt number increased with decreasing of the thickness of the partition due to domination of the convection mode of heat transfer. There was no strong effect of location of the partition on heat transfer at the bottom and top sides of the partition as given in Fig. 7 (d).

Mean Nusselt numbers are presented in Fig. 8 (a) to (f). Actually, the left and right columns can be compared in the same segment in order to clarify the results. Thus, Fig. 8 (a) and (d) gives effects of thermal conductivity on heat transfer with Rayleigh number. The figures indicate that heat transfer increased with increasing of Rayleigh number depending on thermal conductivity. Heat transfer has an increasing function of thermal conductivity. Thus, more heat was transferred from bottom to top. It was noticed that heat transfer became constant for higher values of thermal conductivity. Fig. 8 (b) and (e) can be compared with each other to show the effects of

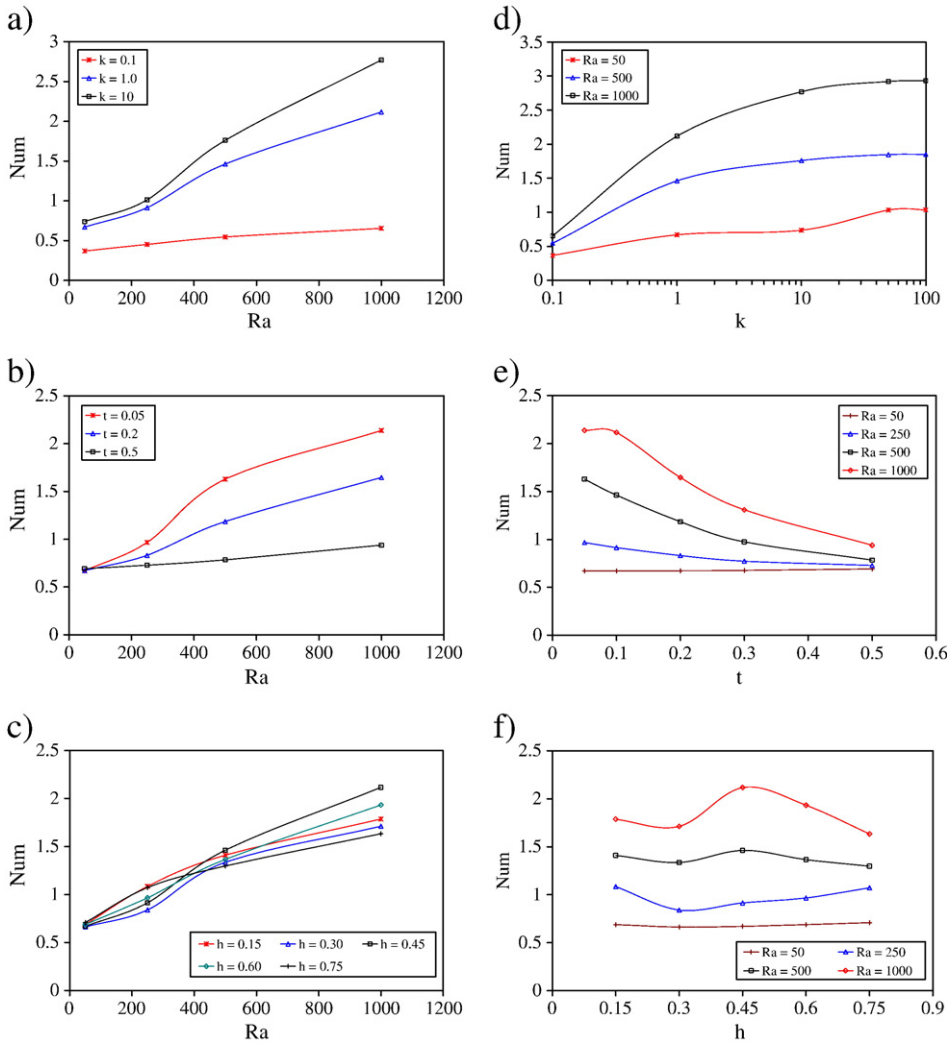

Fig. 8. Variation of mean Nusselt numbers: a) with Rayleigh number for different thermal conductivity ratios at $t=0.1$ and $h=0.45$, b) with Rayleigh number for different dimensionless thicknesses of the partition at $k=1$ and $h=0.45$, c) with Rayleigh number for different dimensionless locations of partition at $k=1$ and $t=0.1$, d) with thermal conductivity ratio for different Rayleigh numbers at $t=0.1$ and $h=0.45$, e) with dimensionless thickness of the partition for different Rayleigh numbers at $k=1$ and $h=0.45$, and f) with dimensionless location of partition for different Rayleigh numbers at $k=1$ and $t=0.1$.

partition thickness on heat transfer. In this case, k was taken as a fixed value ($k=1$). For higher thickness of the partition, the heat transfer regime was almost at conduction. For low values of Rayleigh number, thickness of the partition became insignificant. Fig. 8 (c) and (f) shows the effects of location of partition for different Rayleigh numbers. The figure displays that the location of partition parameter became insignificant for low values of Rayleigh number. For $h=0.30$, heat transfer had a minimal value around $Ra=250$. However, when the partition was located near the top or bottom wall, higher heat transfer occurred around the same value of Rayleigh number. As an interesting result, the heat transfer had a maximum point for $h=0.45$ for higher Rayleigh numbers. It means that heat transfer was mostly with convection when the partition was located at the middle of the cavity. Globally, the results showed that increasing of Rayleigh number enhanced the heat transfer for the same effective parameters.

5. Conclusions

In this numerical work, natural convection in a partially divided porous trapezoidal cavity for a wide range of the governing parameters for non-uniformly heated wall conditions was examined. In the view of the results presented, the main findings can be summarized as follows:

- Heat transfer increases with increasing of Rayleigh number and thermal conductivity ratio.
- Location of the partition becomes insignificant for low values of the Rayleigh number.
- Location of partition is more effective when the partition is located near either the top or bottom wall.
- The heat transfer decreases with increasing of partition thickness due to domination of conduction mode of heat transfer.
- For huge values of thermal conductivity, heat transfer becomes constant inside the enclosure.
- The partition is a control parameter for flow field and temperature distribution. Number of eddies is an independent parameter from all effective parameters. However, their turns or changes in their rotation depend on the parameters.

References

[1] D.B. Ingham, I. Pop (Eds.), Transport Phenomena in Porous Media, Vol. III, Elsevier, Oxford, 2005.
[2] D.A. Nield, A. Bejan, Convection in Porous Media, third ed.Springer, New York, 2006.
[3] D.B. Ingham, A. Bejan, E. Mamut, I. Pop, Emerging Technologies and Techniques in Porous Media, Kluwer, Dordrecht, 2004.
[4] K. Vafai (Ed.), Handbook of Porous Media, second ed., Taylor & Francis, New York, 2005.
[5] T.S. Lee, Numerical experiments with fluid convection in tilted nonrectangular enclosures, Numer. Heat Transfer A 19 (1991) 487–499.
[6] I.E. Sarris, I. Lekakis, N.S. Vlachos, Natural convection in a 2D enclosure with sinusoidal upper wall temperature, Numer. Heat Transfer A 42 (2002) 513–530.
[7] N.H. Saeid, Natural convection in porous cavity with sinusoidal bottom wall temperature variation, Int. Comm. Heat Mass Transfer 32 (2005) 454–463.
[8] Y. Varol, H.F. Oztop, I. Pop, Numerical analysis of natural convection for a porous rectangular enclosure with sinusoidally varying temperature profile on the bottom wall, Int. Comm. Heat Mass Transfer 35 (2008) 56–64.
[9] B.V.R. Kumar, B. Kumar, Parallel computation of natural convection in trapezoidal porous enclosures, Math. Comput. Simul. 65 (2004) 221–229.
[10] A.C. Baytas, I. Pop, Natural convection in a trapezoidal enclosure filled with a porous medium, Int. J. Eng. Sci. 39 (2001) 125–134.
[11] F. Moukalled, S. Acharya, Natural convection in trapezoidal cavities with baffles mounted on the upper inclined surfaces, Numer. Heat Transfer A 37 (2000) 545–565.
[12] F. Moukalled, M. Darwish, Natural convection in a partitioned trapezoidal cavity heated from the side, Numer. Heat Transfer A 43 (2003) 543–563.
[13] M. Peric, Natural convection in trapezoidal cavities, Numer. Heat Transfer A 24 (1993) 213–219.
[14] J.T. Van Der Eyden, T.H. Van Der Meer, K. Hanjalic, E. Biezen, J. Bruining, Double-diffusive natural convection in trapezoidal enclosures, Int. J. Heat Mass Transfer 41 (1998) 1885–1898.
[15] M. Boussaid, A. Djerrada, M. Bouhadef, Thermosolutal transfer within trapezoidal cavity, Numer. Heat Transfer A 43 (2003) 431–448.
[16] S. Kumar, Natural convective heat transfer in trapezoidal enclosure of box-type solar cooker, Renewable Energy 29 (2004) 211–222.
[17] E. Papanicolaou, V. Belessiotis, Double-diffusive natural convection in an asymmetric trapezoidal enclosure: unsteady behavior in the laminar and the turbulent-flow regime, Int. J. Heat Mass Transfer 48 (2005) 191–209.
[18] M. Hammami, M. Mseddi, M. Baccar, Numerical study of coupled heat and mass transfer in a trapezoidal cavity, Eng. Appl. Comp. Fluid Dyn. 1 (2007) 216–226.
[19] Y. Varol, H.F. Oztop, I. Pop, Numerical analysis of natural convection in an inclined trapezoidal enclosure filled with a porous medium, Int. J. Thermal Sci. 47 (2008) 1316–1331.
[20] Y. Varol, H.F. Oztop, I. Pop, Natural convection in right-angle porous trapezoidal enclosure partially cooled from inclined wall, Int. Comm. Heat Mass Transfer 36 (2009) 6–15.
[21] Y. Varol, H.F. Oztop, I. Pop, Maximum density effects on buoyancy-driven convection in a porous trapezoidal cavity, Int. Comm. Heat Mass Transfer 37 (2010) 401–409.
[22] E. Natarajan, T. Basak, S. Roy, Natural convection flows in a trapezoidal enclosure with uniform and non-uniform heating of bottom wall, Int. J. Heat Mass Transfer 51 (2008) 747–756.
[23] H. Asan, L. Namli, Numerical simulation of buoyant flow in a roof of triangular cross-section under winter day boundary conditions, Energy Build. 33 (2001) 753–757.
[24] P.M. Haese, M.D. Teubner, Heat exchange in an attic space, Int. J. Heat Mass Transfer 45 (2002) 4925–4936.
[25] A.C. Baytas, I. Pop, Free convection in oblique enclosures filled with a porous medium, Int. J. Heat Mass Transfer 42 (1999) 1047–1057.